AN ANALYSIS OF THE PRESSURE TRANSIENT TESTING OF A MAN-MADE FRACTURED GEOTHERMAL RESERVOIR *

by

Henry N. Fisher and Jefferson W. Tester
Group G-3, MS 981
Los Alamos Scientific Laboratory
Los Alamos, NM 87545

Submitted to:

Stanford Workshop on Geothermal Reservoir Engineering
December 12, 1979

ABSTRACT

Pressure-transient testing of a hydraulically fractured geothermal reservoir in low-permeability crystalline basement rock has involved constant rate injection and pressure buildup tests under a wide range of field conditions for a number of fractured regions. Following conventional reservoir analysis methods, data are treated in terms of a transient diffusion equation that relates fluid flow and pressure levels in the main fracture system, associated joints, and the matrix permeability. Pressure-flow data are compared to type curve solutions of the diffusion equation for various flow geometries. The following points are considered in detail: 1) The limits on the fracture geometry, aperture and diffusing areas as determined from the diffusion parameters. 2) The parameters (flow impedance, diffusivity) of the flow-through systems are related to those governing the pressure inflation of the main fractures. 3) The relationship of the rock properties to the reservoir compressibility, effective porosity and permeability are discussed. In particular, laboratory experiments show that the flow properties of all sizes of cracks from large single fractures to the microstructure are pressure dependent if the fluid pressure is near the confining stress. 4) The competition of flow into the various types of porosity (main fractures, joints, and microstructure) and the effect on the interpretation of type curves are discussed.

INTRODUCTION

A Hot Dry Rock (HDR) geothermal reservoir consisting of fractures connecting two wellbores (GT-2 and EE-1) at Fenton Hill, New Mexico was first established in October, 1975. The fracture system, which is located in low-permeability granite at a depth of approximately 2900 meters, has been altered since then by two redrilling operations in the production hole (GT-2) and subsequent hydraulic fracturing attempts in both EE-1 and GT-2.

*Work performed under the auspices of the U.S. Department of Energy.

Many experiments involving the pressurization of one or both boreholes from which the fracture originates have also changed the flow characteristics of the system. These experiments have continued to give information on the permeation flow into the surrounding rocks, the properties of the reservoir rock, the geometry and extent of the main fractures, and the flow through properties of the heat exchange paths.

The field reservoir is shown schematically in Fig. 1. Detailed descriptions of the drilling history are provided in refs. 1 through 5. Briefly, the chronology is as follows. GT-2 was drilled first to a depth of 2.929 km and cased to 2.917 km. Hydraulic fracturing experiments produced a fracture system with the main exit from the wellbore at 2.81 km. EE-1 was drilled to a depth of 3.06 km but did not intercept the main fracture system of GT-2 because of directional drilling problems. Subsequent hydraulic fracturing of EE-1 produced several injection zones with the main exit at 2.76 km, but did not produce a low impedance connection to GT-2. Two further attempts to obtain a low impedance (<15 bar-s/ℓ) connection were made by cementing off and redrilling GT-2A and GT-2B (Fig. 1). Hydraulic fracturing experiments in GT-2A again did not produce the desired impedance. However, GT-2B did produce a connection with a low enough impedance to permit long-term heat extraction and flow tests under a variety of borehole pressurization conditions.

The data available is from two main types of experiments. Injection tests were done on the four wellbores with the other active well shut in. These consist mainly of constant flow or step flow tests; and, the majority were injection into EE-1. They include the attempts at massive hydraulic fracturing. Second, circulation tests were usually performed by pumping into EE-1 and producing through the active branch of GT-2 (see Fig. 1). The GT-2 wellhead pressure was most often maintained near zero (hydrostatic); the notable exception was a high back-pressure flow test between EE-1 and GT-2B with GT-2B pressurized to near the effective confining stress.

Pressurization of the reservoir can result in water storage in or permeation through several different types of pores or fractures. The small scale porosity associated with the grain boundaries has been examined using core specimens in the laboratory (Refs. 6 through 8) with Hassler-type equipment. These core or matrix porosities are of the order 10^{-3} and the associated permeabilities from 10^{-19} to 10^{-20} m^2 (0.1 to 0.01 μdarcy) under the confining stresses typically encountered in the reservoir.

Considerable natural jointing is observed in the cores and in wellbores (Refs. 1 and 4). These joints have many orientations and spacing of centimeters to meters and are usually sealed with calcite in the normal condition. Possibly, opening of these joints by pressurization can increase the effective permeability to 2×10^{-17} m^2 (Ref. 3). This and the small scale porosity could be initially homogeneous throughout the reservoir; but there is no certainty, especially for the large scale jointing. Flow in the naturally occurring porosity may also be anisotropic. The orientation

of the large joints is not necessarily isotropic and anisotropic earth stresses can induce anisotropic flow properties.

The naturally occurring porosity and joints can be altered by the pressurization and flow of the system and new fractures can be created. The extent to which altered existing joints and new fractures compete to determine the dominate characteristics of the system is not yet known. However, new fractures are expected to be perpendicular to the minimum earth stress and the existing fractures that are nearly perpendicular to the minimum earth stress are expected to open most readily under pressure and may become important flow paths. In any event, the pressurization of the four wellbores produced an extensive, anisotropic, and heterogeneous reservoir. The inflation, and possibly the flow-through characteristics, of the EE-1/GT-2B system, were determined in part by the presence of the GT-2 and GT-2A fractures and their connections to EE-1.

As in conventional reservoir analysis, the model describing the system is based on a diffusion equation for pressure derived from a Darcy-type flow law and the conservation of mass. The early in situ data (Refs. 3, 4, and 5) and laboratory experiments on small scale porosity (Refs. 6, 7, and 8) and on large single fractures (Refs. 9, 10 and 11) necessitated the use of pressure-dependent permeabilities and system compressibilities. This model has provided reasonable fits to the data examined thus far (Refs. 4 and 5).

MATHEMATICAL MODEL

It is assumed here that the average flow velocity is determined by the Darcy equation,

$$\bar{v} = - \frac{k}{\mu} \nabla P \qquad (1)$$

where k is the permeability tensor, μ the fluid viscosity and P the pore pressure. The continuity equation is

$$\nabla \cdot (\rho \bar{v}) = \frac{\partial(\rho\theta)}{\partial t} = 0 \ , \qquad (2)$$

with ρ the fluid density and θ the porosity. Equation (2) can be rewritten using Eq (1) to obtain the diffusional form of the pressure equation:

$$\nabla \cdot \left(\frac{\rho k}{\mu} \nabla P \right) = \frac{\partial(\rho\theta)}{\partial t} = \frac{d(\rho\theta)}{dP} \frac{\partial P}{\partial t} \ . \qquad (3)$$

The fluid density can be expanded as $\rho = \rho_0(1+\beta_w P)$; and by using the compressibility of water $\beta_w \simeq 5.0 \times 10^{-4}$ MPa^{-1}, the following simplification results,

$$\frac{d(\rho\theta)}{dP} = \theta\beta_w\rho_o + \rho_o \frac{d\theta}{dP} . \quad (4)$$

Here, $d\theta/dP$ depends on the bulk properties of the rock, which is about twenty times less compressible than water. So it is not clear which term, if either, of Eq. (4) will dominate depending on the magnitude of θ. Similar considerations hold for the left hand side of Eq. (3). Because of the low porosities expected, the term $\theta\beta_w\rho_o$ in Eq. (4) should not dominate and that ρ can be considered constant. This assumption must be justified later. These assumptions result in a simplification of Eq (3) to:

$$\nabla \cdot (k\nabla P) = \mu \frac{d\theta}{dP} \frac{\partial P}{\partial t} . \quad (5)$$

The related quantities k, θ, and $\beta \equiv d\theta/dP$, and in particular their dependence on pressure cannot be determined exactly since they also depend on the pore volumes, shapes, orientations, and distribution in space, which are, in general, not known. In addition, each depends on the three components of stress, which in turn are determined by the <u>in situ</u> earth stresses and, to some extent, the pore pressure.

Equation (5) has been solved numerically with the finite element AYER code (Ref. 12). The <u>in situ</u> data were matched by developing empirical equations to describe the pressure-dependences of θ, k, and β (Ref. 3 and 4). The pressure-dependence of these empirical expressions also fit laboratory data on the GT-2 cores reasonably well (Refs. 4 and 5).

The porosity is assumed to be controlled by the minimum earth stress σ_3,

$$\theta = \frac{\theta_o^*}{[1-C(\sigma_3+P)]^\alpha} . \quad (6)$$

The permeability tensor is assumed to have three non-zero components. The two components perpendicular to the least horizontal stress are

$$k_3 = \frac{k_o^*}{[1-C(\sigma_3+P)]^{3\alpha}} . \quad (7)$$

The component parallel to the least stress is

$$k_2 = \frac{k_o^*}{[1-C(\sigma_2+P)]^{3\alpha}} . \quad (8)$$

where θ_o^* and k_o^* are evaluated at $\sigma_3+P=0$.

where σ_2 is the intermediate horizontal stress. For the data considered, $P < S_3$ the minimum principle earth stress and the following approximations provide accurate fits to the data:

a) $\sigma_3 \simeq S_3$, the minimum earth stress.

b) $\sigma_2 \simeq S_2$, the intermediate earth stress.

c) $\alpha \simeq 0.6$ (determined parametrically).

This reduces eqs (6), (7) and (8) to:

$$\theta = \frac{\theta_o}{(1-C_3P)^{0.6}} , \tag{9}$$

$$k_3 = \frac{k_o}{(1-C_3P)^{1.8}} , \tag{10}$$

$$k_2 = \frac{k_o}{(1-C_2P)^{1.8}} , \tag{11}$$

and

$$\frac{d\theta}{dP} = \frac{\partial\theta}{\partial P} = \beta = \frac{\beta_o}{(1-C_3P)^{1.6}} . \tag{12}$$

Here,

$$C_3 = \frac{C}{1-CS_3} ,$$

$$C_2 = \frac{C}{1-CS_2} , \tag{13}$$

and θ_o, k_o, and β_o are evaluated at P=0 (the hydrostatic condition).

IN-SITU DATA FITS

The first detailed computer fits to the Fenton Hill pressure and flow data were produced with AYER using solutions to Eq (5) on a two-dimensional grid with the diffusional properties given by Eqs. (9)-(11). As longer flow periods were examined, however, it was found that two-dimensional effects were not observed. Also, no flow dependence was included with only linear,

Darcy-like effects modeled. Only recently has the role of flow dependence been apparent, after the accumulation of much data.

These circumstances have resulted in the determination of the characteristics of a limited number of flow parameters. The early-time inflation data is determined entirely by the parameter $\alpha = A\sqrt{k\beta}$. This parameter results from fits during the one-dimensional, linear flow period where pressure varies directly with the $\sqrt{t}$ at constant injection rate or injection rate decreases linearly with $1/\sqrt{t}$ at constant injection pressure. In this case, the pressure dependence of k and β is only seen in the initial values of $k(P(t=0))$ and $\beta(P(t=0))$. The time constant for the conversion from one-dimensional to multidimensional flow, $\tau_A = A\mu\beta/k$, has not been measured but lower limits have been obtained. For interference or flow-through tests, the time constant for flow or pressurization between wells, $\tau_\ell = \ell^2\mu\beta/k$, and the flow impedance, $I = \Delta P/Q = \ell\mu/Ak$, are determined. The discussion of how important fracture or rock properties are in determining these parameters is discussed later in the paper. For now, we examine only numerical fits to a few selected sets of data to determine the parameter magnitudes and their pressure and flow dependences.

Experiment 111 (Fig. 2) consisted of a pressurization of the injection hole (EE-1) in steps, in constant flow and constant pressure phases (upper curve of Fig. 2). The flow and pressure were recorded in EE-1 and the pressure was recorded in the production hole (GT-2) which was shut in. The fits to the GT-2 pressure (lower curve of Fig. 2) verifies the pressure dependence of β/k. The fits to the EE-1 pressure for the constant flow phases (Fig. 3) give the pressure dependence of $A\sqrt{k\beta}$. However, unless it is assumed that the reservoir is homogeneous, the inflation and flow-through properties are not the same. Because the reservoir is clearly heterogeneous with both fracture and matrix flow important to different sections these parameters are not expected to be measuring the same properties (Ref. 13).

Figure 3 is an example of a pressurization of EE-1 with GT-2 shut-in, first at 2.14 ℓ/s (34 gpm) then at 0.56 ℓ/s (9 gpm). This and longer pressurizations established a lower limit to the time constant for the conversion from one to multidimensional flow.

The same model was used to obtain fits to the water loss data for a 75-day heat extraction experiment (Ref. 13). In this test, the injection wellhead pressure was maintained between 86 and 55 bar while the injection flow rate increased from 7.5 to a maximum of 15.0 liter/sec at the end of the 75-day period. Fluid was continuously produced in GT-2B with a constant surface pressure of ≳10.0 bar. Figure 4 compares the data for the integrated flow into all permeation with the calculated results.

DISCUSSION

Even though the mathematical model provides good fits to much of the data, the resulting empirical diffusion parameters cannot be interpreted

in terms of a unique flow or fracture geometry. From the time of the formation and activation of the first fractures at Fenton Hill it has been assumed that the early time pressure and flow history of the fracture system was determined by permeation flow out of a large low impedance (infinite conductivity) main fracture into the surrounding matrix or joints. Considerable evidence now suggests that much of this early time data can also be adequately characterized by linear flow into and inflation of discrete fractures of moderate impedance.

Consequently, the early time period may be dominated by flow in discrete fractures, whereas at later times flow into the reservoir is controlled by matrix and/or joint permeation. Some of the characteristics of the system that support this view are as follows:

1) No large zero-impedance fracture volume has been detected.
2) The inflation parameters and flow-through parameters can come from fractures that have the same dimensions.
3) The pressure dependence of the inflation and flow-through parameters are the same and agree with those of large fractures examined in the laboratory in other rocks (Ref. 9, 10, and 11).
4) The long-term water loss data implies a large inflated fracture area and small total matrix and joint permeability.

In Fig. 5 an attempt has been made to estimate the average fracture width (small dimension perpendicular to the flow) and the average fracture height (large dimension perpendicular to the flow) for all the fractures connected directly to EE-1 after the 75-day experiment (Ref. 13). All calculations are for a fracture compressibility obtained from the pressure dependence of the impedance. The vertical line labeled $\sqrt{A}$ is the square root of the heat exchange area. The lines labeled V_o=1 m^3 and V=50 m^3 are, respectively, an estimate of the maximum zero impedance fracture volume and the flow-through volume obtained from the dye tracer studies (Ref. 14). The line labeled α_f=300 cm^3 is obtained from a nominal value of the inflation parameter $A_f\sqrt{k_f\beta_f}$ for fracture flow. The dashed lines are obtained from the flow-through impedance for a low EE-1 pressure (Exp. 184) and a high EE-1 pressure (Exp. 190).

Approximate limits can also be obtained for those parameters that determine the long-term water losses of the system. By assuming that the small scale permeability limits the size of the system and by assuming a canonical value of pore compressibility as obtained in the laboratory (β = 4.0 x 10^{-5} MPa^{-1}), an upper limit on the permeating area and on the effective value of permeability can be determined. Figure 6 is a plot of effective permeability confining the system versus the square root of the permeating area. Each straight line represents a limit set by some measured parameter, the allowable portion of the graph is indicated by the

direction of the arrow. The parameters and limits annotated on the figure are:

1) τ_{Λ}: limits set by one-dimensional nature of the flow.
2) $\dot{Q}$: limit set by small value of long-term water loss rate.
3) $\sqrt{A_T}$: limit set by assuming that the permeating area is larger than the heat exchange area.
4) k: limit set by smallest laboratory permeability.
5) $A\sqrt{k\beta}$: limit set by assuming that this parameter is determined only by the small scale porosity.
6) V_V: limit set by approximate venting volumes.

CONCLUSIONS

What we have tried to present in this paper is an objective discussion of a classic non-uniqueness problem that faces us in the intepretation of our pressure-transient data. The deployment of infinite and finite fracture conductivity models with linear flow and pressure-dependent properties is a departure from the more conventional reservoir engineering approaches which assume homogeneous and constant properties for k, θ, and β. Type-curve fits from such approaches are inadequate, causing us to develop numerical simulations with empirical representations of pressure-dependent effects.

REFERENCES

1. A. G. Blair, J. W. Tester, and J. J. Mortensen, "LASL Hot Dry Rock Geothermal Project, July 1, 1975-June 30, 1976," Los Alamos Scientific Laboratory report LA-6525-PR (October 1976).

2. H. D. Murphy, R. G. Lawton, J. W. Tester, R. M. Potter, D. W. Brown, and R. L. Aamodt, "Preliminary Assessment of a Geothermal Energy Reservoir Formed by Hydraulic Fracturing," Soc. Pet. Eng. 17, 317-326 (August 1977).

3. H. N. Fisher, "An Interpretation of the Pressure and Flow Data for the Two Fractures of the Los Alamos Hot Dry Rock (HDR) Geothermal System," Proc. of the 18th U.S. Symposium on Rock Mechanics, Keystone, CO., (June 22, 1977).

4. LASL HDR Project Staff, "Hot Dry Rock Geothermal Energy Development Project, Annual Report, Fiscal Year 1977," Los Alamos Scientific Laboratory report LA-7109-PR (February 1978).

5. M. C. Brown, et al, "Hot Dry Rock Geothermal Energy Development Program, Annual Report Fiscal Year 1978," Los Alamos Scientific Laboratory report LA-7807-HDR (April 1979).

6. R. Trice and N. Warren., "Preliminary Study on the Correlations of Acoustic Velocity and Permeability in Two Granodiorites From the LASL Fenton Hill Deep Borehole," LA-6851-MS, Los Alamos Scientific Laboratory, Los Alamos, NM (July 1977).

7. J. M. Potter, "Experimental Permeability Studies at Elevated Temperature and Pressure of Granite Rocks," Los Alamos Scientific Laboratory report LA-7224-T (May 1978).

8. C. J. Duffy, "Permeability, Porosity, and Pore Compressibility" in "Hot Dry Rock Geothermal Energy Development Program Annual Report Fiscal Year 1978," Los Alamos Scientific Laboratory report LA-7807-HDR, p 63-68 (April 1979).

9. P. A. Witherspoon, et al, "Stress-Flow Behavior of a Fault Zone with Fluid Injection and Withdrawal," University of California, Report No. 77-1 (May 1977).

10. R. L. Kranz, et al, "The Permeability of Whole and Jointed Barre Granite," Int. J. Rock Mech. Min. Sci. and Geomech. Abstr. Vol. 16, pp 225-234 (August 1979).

11. H. R. Pratt, et al, "Elastic and Transport Properties of an In Situ Jointed Granite," Int. J. Rock Mech. Min. Sci. and Geomech. Abstr. Vol. 14, pp 35-45 (1977).

12. R. G. Lawton, "The AYER Heat Conduction Computer Program," Los Alamos Scientific Laboratory report LA-5613-MS (May 1974).

13. J. W. Tester and J. N. Albright (Eds.), "Hot Dry Rock Energy Extraction Field Test: 75 Days of Operation of a Prototype Reservoir at Fenton Hill," LA-7771-MS, Los Alamos Scientific Laboratory, Los Alamos, NM (April 1979).

14. J. W. Tester, R. M. Potter, and R. L. Bivins, "Interwell Tracer Analyses of a Hydraulically Fractured Granite Geothermal Reservoir," paper SPE 8270 presented at SPE-AIME 54th Annual Fall Technical Conference and Exhibition, Las Vegas, NV (Sept. 23-26, 1979).

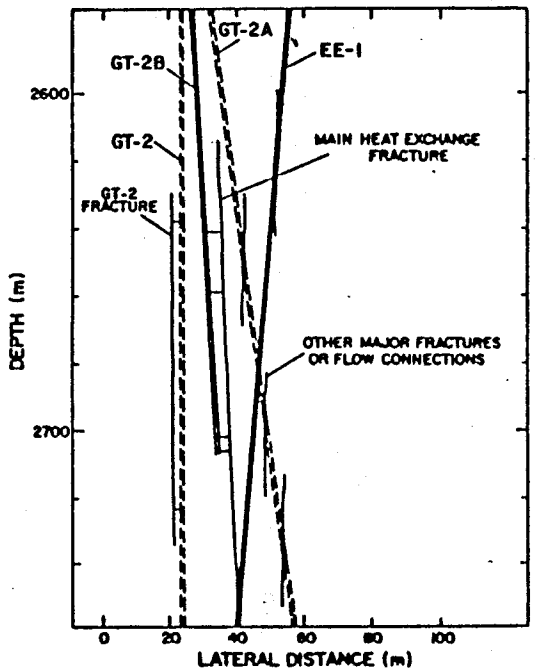

FIG. 1: SCHEMATIC OF FENTON HILL RESERVOIR

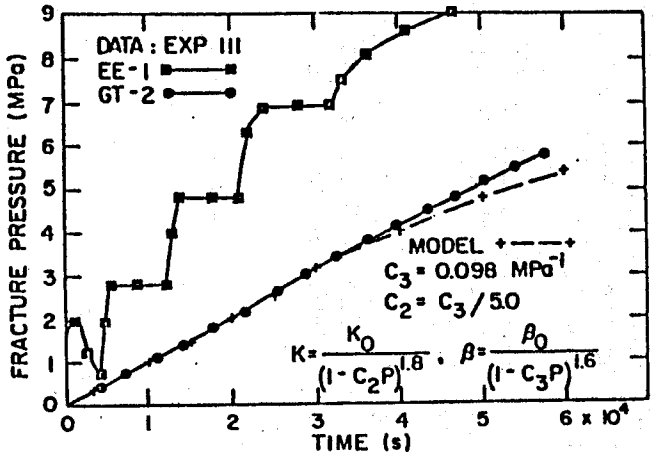

FIG. 2: FRACTURE PRESSURES DURING EXPERIMENT III

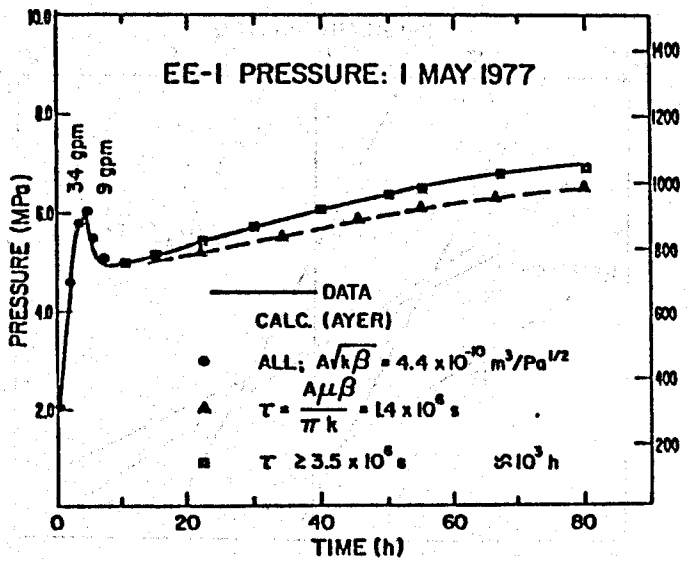

FIG. 3: EE-1 PRESSURE DURING MAY 1, 1977 PUMP-UP

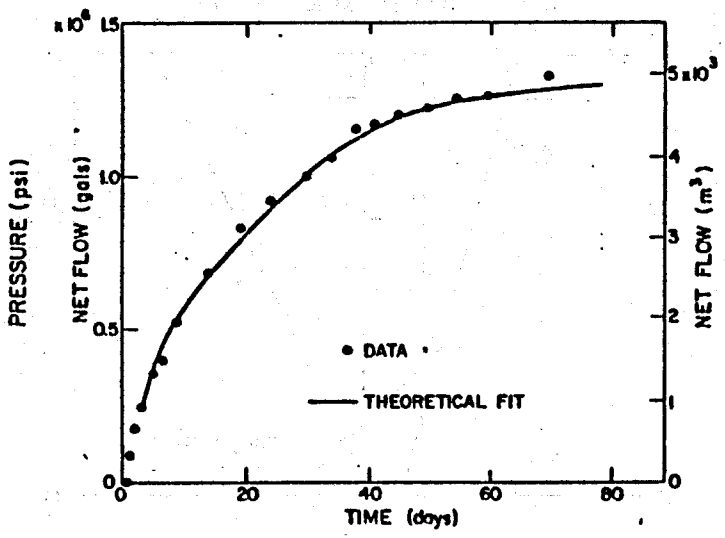

FIG. 4: NET WATER LOSS DURING 75-DAY TEST

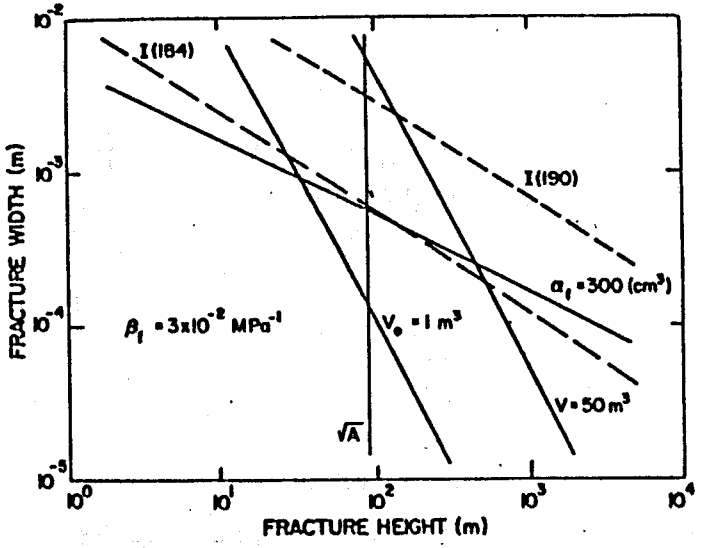

FIG. 5: APPROXIMATE FRACTURE DIMENSIONS AFTER 75-DAY TEST

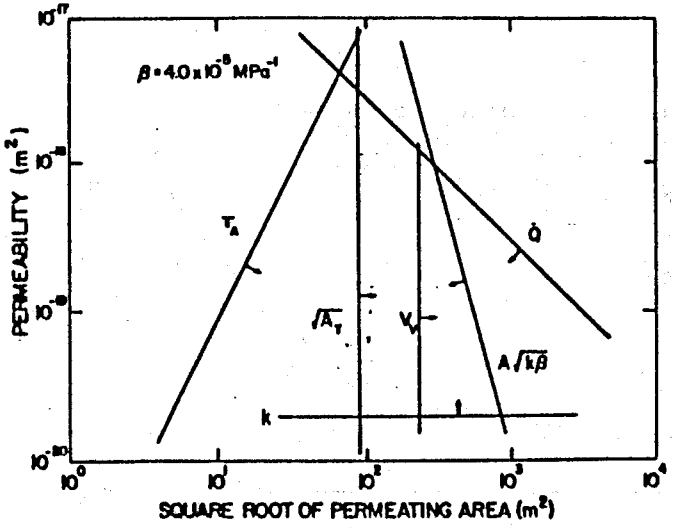

FIG. 6: LIMITS ON PERMEABILITY AND PERMEATING AREA SET BY LONG-TERM FLOW DATA